Available online at www.sciencedirect.com

SciVerse ScienceDirect

Ceramics International 38 (2012) 5563–5570

CERAMICS INTERNATIONAL

www.elsevier.com/locate/ceramint

Raman spectra, photoluminescence and ferromagnetism of pure, Co and Fe doped SnO_2 nanoparticles

Jasneet Kaur [a], Jyoti Shah [b], R.K. Kotnala [b], Kuldeep Chand Verma [a,*]

[a] Department of Physics, Eternal University, Baru Sahib, Sirmour, HP 173101, India
[b] National Physical Laboratory, New Delhi 110012, India

Received 1 January 2012; received in revised form 29 March 2012; accepted 30 March 2012
Available online 6 April 2012

Abstract

The pure and transition metal (Co and Fe = 3 and 5 mol%) doped SnO_2 nanoparticles have been synthesized by a chemical route using polyvinyl alcohol as surfactant. These nanoparticles were characterized by X-ray diffraction (XRD), transmission electron microscopy (TEM), Raman, Fourier transform infrared (FTIR) spectroscopy, photoluminescence (PL) and magnetic measurements. The XRD patterns show that all the samples have tetragonal rutile structure without any extra phase and the value of average particle size using FWHM lies within 12–29 nm is also confirmed by TEM. FTIR spectrum has been used to confirm the formation of Sn–O bond. Raman spectroscopy shows the intensity loss of classical cassiterite SnO_2 vibration lines which is an indication of significant structural modifications. From PL, an intense blue luminescence centered at a wavelength ~530 nm is observed in the prepared SnO_2 nanoparticles, which is different from the yellow-red light emission observed in SnO_2 nanostructures prepared by other methods. The strong blue luminescence from the as-grown SnO_2 nanoparticles is attributed to oxygen-related defects that have been introduced during the growth process. These Co and Fe-doped SnO_2 nanoparticles exhibit room temperature ferromagnetism and the value of their magnetic moment and phase transition temperature are sensitive to their size and stoichiometric ratio.

Keywords: A. Sol–gel processes; B. Electron microscopy; E. Spintronics; Magnetic and optical properties; SnO_2

1. Introduction

Ferromagnetism of dilute magnetic semiconductors (DMSs) has been a subject of recent investigations because of their potential applications in the emerging fields such as spintronics, nanoelectronics, nanophotonics, magneto electronics and microwave devices [1,2]. A wide band gap oxide based DMSs such as TiO_2, ZnO, SnO_2, and HfO_2 have attracted considerable attention whenever doped with transition metal (TM) ions (Co, Mn, Ni, Fe, Cr, etc.) because their remarkable electronic, optical and magnetic properties resulting from a large sp–d exchange interactions between the magnetic ions and the band electrons.

Among above DMSs oxides, SnO_2 is an important n-type semiconductor of wide energy gap (E_g = 3.62 eV at 300 K) and presents special properties, such as transparency, chemical and thermal stabilities which are used in photodetectors, catalysts for oxidation and hydrogenation, solar cells, semiconducting gas sensors, liquid crystal displays, protective coatings, etc. [3,4]. There are a lot of works have been reported on ferromagnetic properties of TM-doped SnO_2 thin films and nanoparticles. Ogale et al. [5] reported room-temperature ferromagnetism of pulsed laser deposited SnO_2:Co thin films. More recently, Fitzgerald et al. [6] found ferromagnetism in Co-doped SnO_2 thin films with Co contents from 0.1 to 15%. On the other hand ferromagnetism of $Sn_{0.95}Fe_{0.05}O_2$ ceramic with magnetic moment of 0.95 μ_B/Fe, about 85% of the iron being in a magnetically order high-spin Fe^{3+} and Curie temperature of about 360 K were reported by Fitzgerald et al. [7]. However, Punnoose et al. [8] reported the paramagnetic behavior of chemically synthesized $Sn_{0.95}Fe_{0.05}O_2$, prepared above 600 °C and Adhikari et al. [9] observed antiferromagnetic behavior of 5% Fe-doped SnO_2 nanoparticles synthesized by chemical co-precipitation method. Overall, the origin of ferromagnetism in TM doped SnO_2 system is still an open issue.

* Corresponding author. Tel.: +91 9418941286; fax: +91 1799276006.
E-mail addresses: jasneet.physics@gmail.com (J. Kaur), kuldeep0309@yahoo.co.in (K.C. Verma).

0272-8842/$36.00
http://dx.doi.org/10.1016/j.ceramint.2012.03.075

Nanometric size has great influence on the performance of several material systems and may affect various physical properties not only the host semiconductors but also of the DMS materials derived from them. For example, when the crystallite size in some of the DMS materials is reduced below 30 nm, they are found to exhibit better ferromagnetic properties as compared with those having microcrystalline particles (>100 nm) [10]. In addition, nanocrystalline oxide DMSs may be exploited for a variety of applications such as spintronic devices, biomedical applications, magnetic storage devices, and ferrofluids. DMSs SnO_2 also exhibits remarkable features such as native oxygen vacancies, high carrier density and transparency, and high chemical and thermal stabilities. A fewer studies [3,6,8,11] on nanocrystalline Co and Fe-doped SnO_2 DMSs with conflicting results especially on the existence of room temperature ferromagnetism have been reported. In view of above these discussions there is need for appropriate growth conditions which results to obtain room temperature ferromagnetism.

Moreover, bulk SnO_2 is a member of special class semiconductors which have direct band gaps and dipole forbidden due to their special wave function symmetry. Therefore, to pursue the potential for light emission near band edge, researchers have paid more attention to explore the luminescence properties of nanostructures, expecting that nanostructured materials may break the selection rule imposed on their bulk counterparts [12,13]. SnO_2 nanostructures showed broad emissions in the wavelength range of 400–600 nm at room temperature which is related to the deep level defects [14].

There are several methods used by researchers to prepare DMS SnO_2 such as chemical co-precipitation, conventional mixed oxide, sol–gel, and hydrothermal process [15,16]. However, most of them have been directed toward the preparation of particles with a large size distribution of few micrometers economically, despite complicated experimental steps and high reaction temperatures. In the present paper, we have prepared Co and Fe-doped SnO_2 nanoparticles by sol–gel method in which polyvinyl alcohol (PVA) is used as surfactant and the resulting size of the prepared nanoparticles is comparatively smaller and the quality is even better. We have prepared samples of pure SnO_2 (S0), $Sn_{0.97}Co_{0.03}O_2$ (SC3), $Sn_{0.95}Co_{0.05}O_2$ (SC5), $Sn_{0.97}Fe_{0.03}O_2$ (SF3), $Sn_{0.95}Fe_{0.05}O_2$ (SF5) nanoparticles. The Raman shifts support the existing phase structure and nano effect of TM doped SnO_2. The PL spectra depict its optical nature and exhibit an intense blue luminescence. The magnetic properties depend not only on the oxygen vacancies but also on electronic and structural modifications and the surface nature of the nano crystallites.

2. Experimental procedure

Pure and doped SnO_2 nanoparticles were prepared by a chemical route using PVA as surfactant. The precursor solutions were prepared from stannic chloride pentahydrate ($SnCl_4{\cdot}5H_2O$), ferric chloride ($FeCl_3$) and cobalt chloride ($CoCl_2{\cdot}6H_2O$) with desired molar concentration. In this method, ethanol and acetic acid were mixed in the ratio of 3:1. $SnCl_4{\cdot}5H_2O$ was added to it and stirred for 2 h on a magnetic stirrer. In this solution a calculated amount of dopants Co and Fe was added and again stirred for 1 h. The precursor solutions (M) were mixed in PVA solution in the molar ratio of M:PVA::5:2. The solution was dried at 250 °C and annealed at 700 °C for 2 h to crystallize. The reaction mechanism of PVA with metal ions ($M^+ = Sn^{4+}$, Co^{2+}, Fe^{3+} etc.) is shown in Fig. 1. During heating there exist two sites namely hydrophobic (H_b) and hydrophilic (H_p) of PVA and form clusters. The H_b keeps

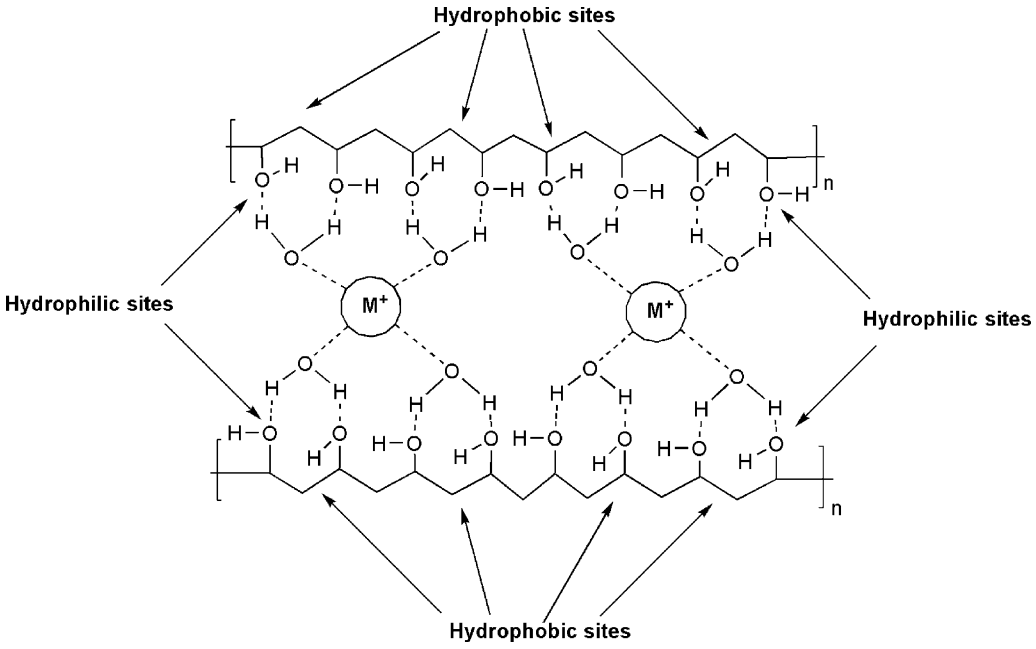

Fig. 1. Mechanism during growth of metal ions in the presence of PVA.

the materials separate due to their repulsive forces which slow down the rate of reaction. Secondly, the H_p keeps the metal intact and retards the growth process. Hence the surfactant PVA helps in synthesizing small sized nanoparticles. The crystalline structure was analyzed by X-ray diffraction (XRD) by using X'Pert PRO PANalytical system and microstructure by transmission electron microscopy (TEM) by using HITACHI H-7500. Fourier transform infrared (FTIR) spectrum was recorded on a Perkin Elmer spectrum 400 FT-IR/FT-FIR spectrometer using triglyceride (TGS) detector. Photoluminescence (PL) and Raman spectrum of the samples was recorded on Renishaw UK which consists of Ar ion laser with 518 nm wavelength and 50 mW power. The magnetic measurement was performed at room temperature using vibrating sample magnetometer (Lakeshore VSM model number 7307).

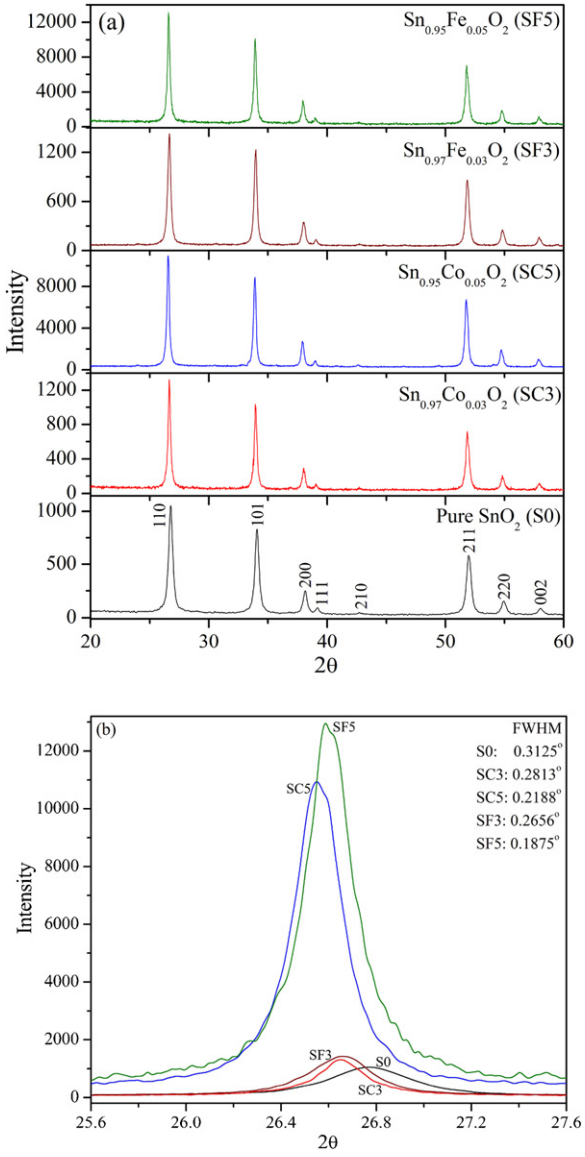

Fig. 2. (a) XRD pattern of pure, Co and Fe doped SnO_2 nanoparticles. (b) XRD pattern between $2\theta = 25.6$ and 27.6°.

3. Results and discussion

XRD patterns of pure, SC and SF nanoparticles are shown in Fig. 2(a). The peaks pointed out at $2\theta = 26.81°$(1 1 0), 34.04°(1 0 1), 38.07°(2 0 0), 39.13°(1 1 1), 42.69°(2 1 0), 51.93°(2 1 1), 54.90°(2 2 0), and 57.98°(0 0 2) correspond to tetragonal SnO_2 rutile structure crystallite ($P4_2/mnm$). The diffraction peaks observed in each sample show that the S0, SC and SF nanoparticles are polycrystalline in nature. No diffraction peaks from Co, Fe or other impurities were detected. XRD pattern also shows that with doping of Co and Fe in SnO_2, the 2θ of diffraction peak shifts slightly to the lower angle and also the full width at half maxima (FWHM) of the diffraction peaks decreases with increasing Co and Fe content [as shown in Fig. 2(b)]. The decrease in FWHM along with an increase in peak intensity suggests that Co and Fe incorporation into the SnO_2 lattice results in an increase in grains size of the doped nanoparticles. The average grains size of the prepared nanoparticles calculated by Scherer relation are 12, 13, 21, 14 and 29 nm, and the tetragonal distortion (c/a) are 0.671, 0.673, 0.676, 0.676 and 0.678, respectively, calculated for S0, SC3, SC5, SF3 and SF5 samples. These values of average grains size, and a and c parameters are given in Table 1. The increment in the values of average grains size and distortion ratio with Co and Fe doping because of the smaller ionic radii of Sn^{4+} (0.69 Å) ion than dopants Co^{2+} (0.72 Å) and Fe^{2+} (0.77 Å) (Fe^{2+} exists because it is ferromagnetic as shown in Fig. 7 whereas Fe^{3+} is paramagnetic [9]). This physical process suggests that a portion of the metal oxide ions formed stable solid solutions with SnO_2 and the metal oxide ions occupy the regular lattice site in SnO_2. Thus, it may lead to the introduction of point defects and change in stoichiometry owing to charge imbalance which leads to a distortion in the crystal structure of the host compound [17]. When the metal oxide ions occupy the regular lattice site in SnO_2, the interference takes place between Co and Fe-doped metal ions and those of SnO_2 lattice, and owing to crystalline behavior of Fe and Co-doped SnO_2 nanoparticles tends to enhance than pure SnO_2. Moreover, the ionic radius of Fe^{2+} (0.77 Å) is larger than Fe^{3+} (0.63 Å) results into increase in grains size when incorporated in Sn^{4+} (0.69 Å) suggests that Fe^{2+} ion exist in the present samples. Thus, the expansion of lattice parameters and the lattice volumes with Fe concentration can be understood by the incorporation of Fe^{2+} ions replacing Sn^{4+} in tetragonal host lattice and similar results were observed by Ghosh et al. [18].

Table 1
Values of lattice parameters a and c, average particles size x from XRD, x' from TEM, saturation magnetization M_s and magnetic phase transition temperature (T_{mp}).

Specimen	a (Å)	c (Å)	x (nm)	x' (nm)	M_s (memu/g)	T_{mp} (K)
S0	4.718	3.168	12	11	Diamagnetic	–
SC3	4.685	3.154	13	12	35.03	447
SC5	4.674	3.161	21	20	120.90	505
SF3	4.711	3.188	14	15	15.09	464
SF5	4.635	3.147	29	30	44.93	513

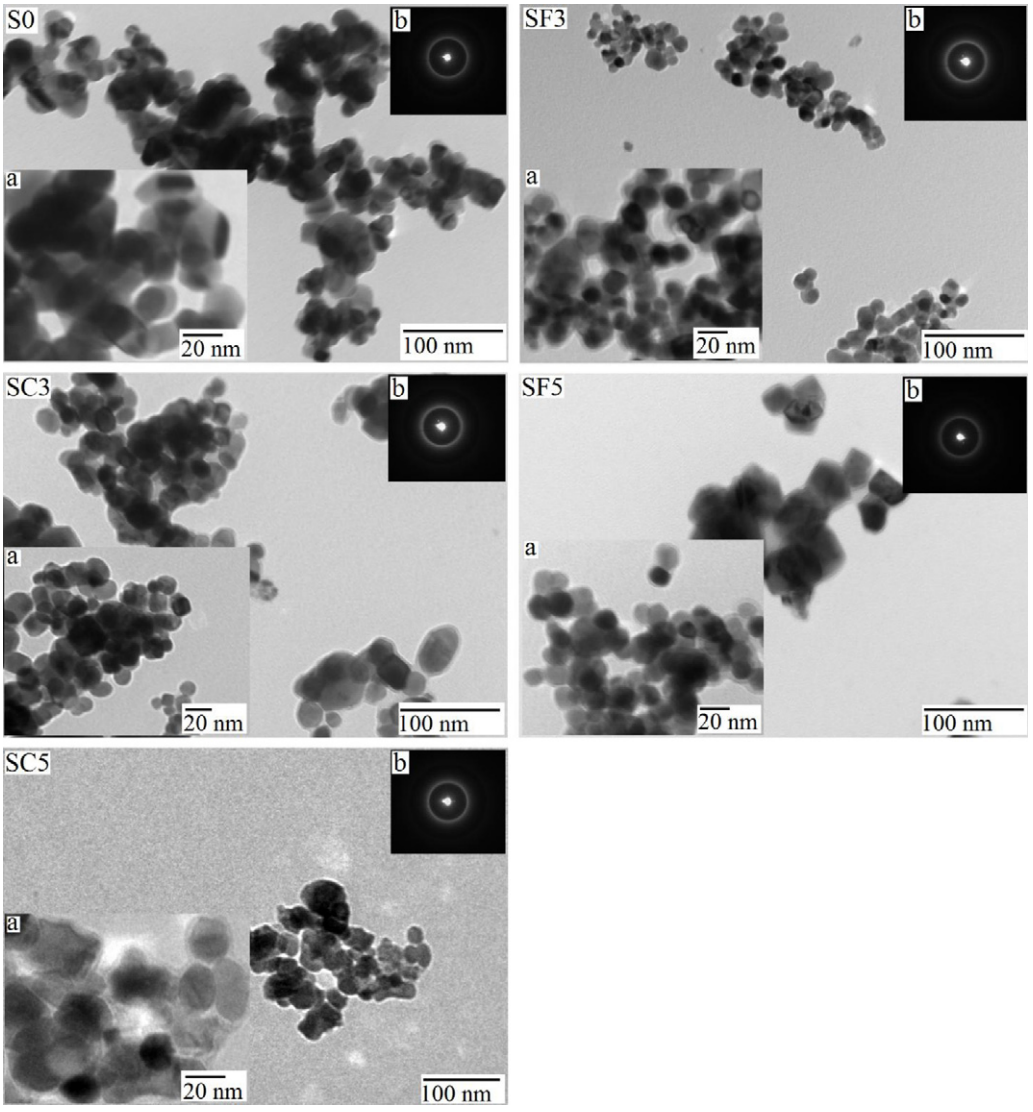

Fig. 3. TEM images. Inset (a) shows images with high magnification and (b) selected area diffraction patterns of the respective sample.

Fig. 3 illustrates the surface morphology of Co and Fe-doped SnO_2 nanoparticles by TEM measurements. Insets (a) and (b) in each sample of Fig. 3 shows the TEM image with high magnification and corresponding selected area diffraction patterns, respectively. These images reveal that the crystalline nature and uniformity of each sample consists of large aggregates which are transformed to more fine aggregates on increasing the dopant concentration. It can also be seen that the average grains size increases with increasing the doping of Co and Fe. The quality of crystallinity is also observed from the selective area diffraction patterns. Most of the particles are tetragonal in shape, and their average grains size is 11, 12, 20, 15 and 30 nm, respectively, for S0, SC3, SC5, SF3 and SF5, which are also given in Table 1. Thus, these values of grains size observed from TEM images are well agreement with those calculated by XRD peaks. The nano fabrication of particles in the samples occurs because PVA is used as a surfactant which slows down the crystal growth process during heating [19].

Fig. 4 shows the FTIR transmittance spectra of Co and Fe-doped SnO_2 nanoparticles involves changes in the positions,

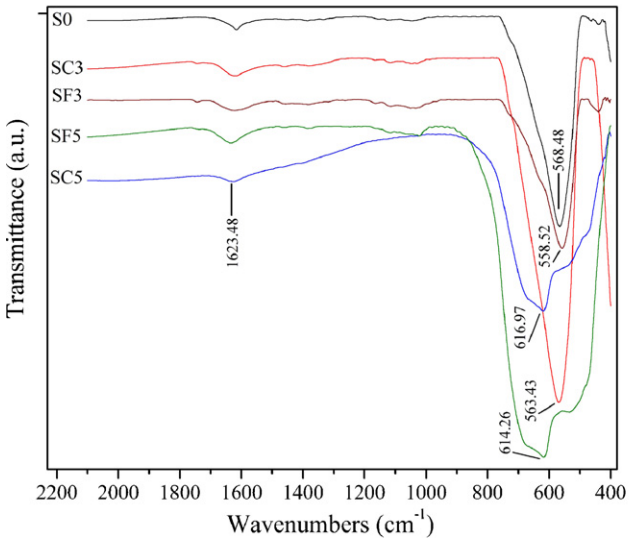

Fig. 4. FTIR analysis of pure, Co and Fe doped SnO_2 nanoparticles.

sizes, and shapes of IR peaks which indicate that the Fe and Co have been incorporated in SnO_2 host. As the spectrum was recorded after heating the samples at 700 °C the presence of vibrations such as O–H and C–H. Characteristic of this region cannot be expected. However the peaks at 1623.48 cm^{-1} are attributed to KBr as used binder during measurements. The bands exhibited in the low wavenumber region 430–620 cm^{-1} relates to the vibration of antisymmetric O–Sn–O bridge functional groups of SnO_2, while a lattice mode due to SnO_2 appears in the region 680–775 cm^{-1}. The peaks appearing at 568.48 (S0), 563.43 (SC3), 616.97 (SC5), 558.52 (SF3) and 614.26 cm^{-1} (SF5) are the characteristic vibration absorption peaks of the Sn–O bond in SnO_2 [20]. By comparing present FTIR spectra with those of microcrystalline SnO_2 [21], one may conclude that the position and the line shapes of nanocrystalline SnO_2 are different from those of microcrystalline ones.

The optical measurements by Raman spectroscopy is an important tool to confirm the substitution of Co and Fe in Sn ions of SC and SF samples and to understand the crystallinity, structural defects, nano metric size effects on vibrational properties, have been performed at room temperature [seen in Fig. 5]. The crystalline quality can be judged from the analysis of the peak shapes and the selection rules. The SnO_2 has a unit cell that consists of two tin and four oxygen atoms. The 6 unit cell atoms give a total of 18 branches for the vibration modes in the first Brillouin's zone. The mechanical representation of the normal vibration modes at the center of the Brillouin's zone is given as [22]:

$$\Gamma = \Gamma_1^+(A_{1g}) + \Gamma_2^+(A_{2g}) + \Gamma_3^+(B_{1g}) + \Gamma_4^+(B_{2g}) + \Gamma_5^-(E_g) + 2\Gamma_1^-(A_{2u}) + 2\Gamma_4^-(B_{1u}) + 4\Gamma_5^+(E_u) \quad (1)$$

The modes A_{1g}, B_{1g}, B_{2g}, and E_g are Raman active while A_{2u} and E_u are infrared active. These Raman spectra are found to be similar to that of pure SnO_2. The most intense peak observed at 630.48 cm^{-1} can be attributed to the A_{1g} mode, which is found to shift to 619.65 cm^{-1} in SC and 624.83 cm^{-1} in SF samples, while those exhibited at 472.4 and 708.23 cm^{-1} may be due to vibrational modes E_g and B_{2g}, respectively. The A_{1g} and B_{2g} modes are non degenerate might be related to the expansion and contraction of the vibrating mode of Sn–O bonds, whereas the doubly degenerate E_g mode may be related to the vibration of oxygen in the oxygen plane. The A_{1g} and B_{2g} modes vibrate in the plane perpendicular to the c-axis, whereas the E_g mode vibrates in the direction of the c-axis.

In addition to these peaks, some extra peaks are observed in S0 nanoparticles at 428.64, 501.57, 768.79 and 860.06 cm^{-1} and the observation of these new peaks can be explained on the basis of the nano effect. In nanocrystalline SnO_2 system, the surface properties are sensitive not only to the grain size and their distributions but also the oxygen vacancies and local disorder so there may be possibility of the appearance of new modes in the Raman spectra [23]. It is interesting to note that by substituting Co and Fe in the SnO_2 lattice, the intensities of all the Raman peaks are found to decrease. This behavior might be due to the fact that the dopants Fe and Co substitution might be responsible for the changes in local disorder and defects such as vacant lattice sites or vacancy cluster or local disorder which may result in lattice distortion and reduction in lattice space symmetry.

Photoluminescence spectroscopy is a suitable technique to determine the crystalline quality, surface defects, energy bands and exciton fine structure. Fig. 6 shows the PL spectrum corresponding to excitation wavelength $\lambda = 514$ nm and the inset show the shift of the emission spectra within a smaller wavelength region 530–561 nm. It may be noted that the pure SnO_2 has an intense blue luminescence centered at 531.13 nm (2.33 eV) is observed in the emission spectra of the SnO_2 nanoparticles and when the dopant concentration increases, the emission peaks shift toward lower wavelength region, i.e., in the high energy region. The observed behavior may be attributed to the fact of incorporation of the dopant in the lattice might have influenced not only the local disorder but also the

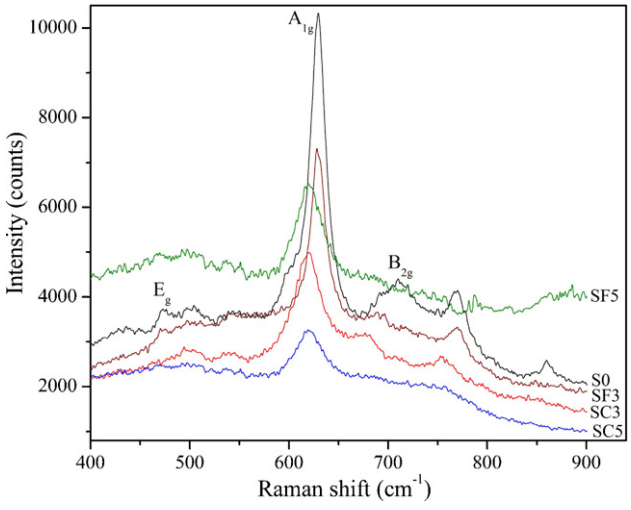

Fig. 5. Raman spectra of pure, Co and Fe doped SnO_2 nanoparticles.

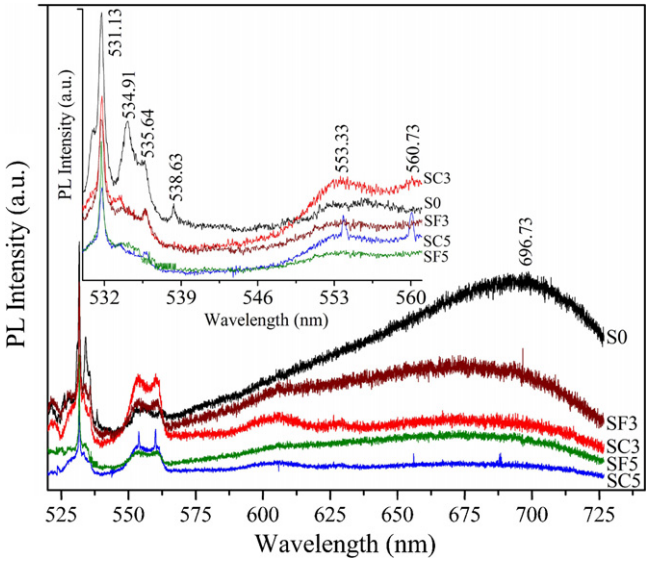

Fig. 6. PL pure, Co and Fe doped SnO_2 nanoparticles. Inset shows PL between smaller wavelength 530 and 561 nm.

positions of oxygen vacancies and their distributions. It should be noted that the strong blue luminescence has been reported before by few researchers [12,24]. However, the blue luminescence from the SnO_2 nanoparticles can be attributed to oxygen-related defects that have been introduced during growth process. Due to the synthesis of SnO_2 nanoparticles in an aqueous solution, a high density of oxygen and tin vacancies [25] is expected which is responsible for the interactions between these oxygen and interfacial tin vacancies, would eventually lead to the formation of a significant number of trapped states. These trapped states thus form a series of metastable energy levels within the band gap result into a strong PL signal at room temperature.

Considering that the energy gap of bulk SnO_2 is 3.62 eV, the emission peaks are lesser than the band gaps of all the samples so they cannot be assigned to direct recombination of a conduction electron in Sn 4p band and a hole in O 2p valence band. Moreover, the nanograins assemblage has large number of defects such as vacancies of oxygen, vacancy clusters, and local lattice disorders at the interface and interior surface of the samples. It can be seen that the strong UV emission peaks are found to vary between 531.13 and 538.63 nm. However, it exhibits a strong broadband luminescence centered at 696.73 (1.78 eV), 607.51 (2.04 eV), 606.01 (2.05 eV), 678.02 (1.83 eV) and 677.22 nm (1.83 eV), respectively, for S0, SC3, SC5, SF3 and SF5 samples exhibit a slightly blue-shifted PL peaks. These peaks may be attributed to crystalline defects induced during growth and the interaction between oxygen vacancies and interfacial tin vacancies which result in a strong PL signal. Another unique feature observed is that there is decrease in emission spectral intensity with the increasing dopant concentration in doped samples. This behavior is attributed to the interaction between the dopant atoms and the support oxide, which is reflected in the reduction of peak intensity.

Fig. 7 shows the room-temperature magnetic properties of Co and Fe-doped SnO_2 nanoparticles. The pure SnO_2 exhibits typical diamagnetic behavior. However, the substitutional incorporation of Co and Fe element into SnO_2 surprisingly transforms the materials from diamagnetic state to ferromagnetic. It is clear that all curves display hysteresis phenomenon at room temperature. The values of saturated magnetization (M_s) are 35.03, 120.90, 15.09 and 44.93 memu/g and coercive field are 322, 40, 101 and 50 Oe, respectively, observed in SC3, SC5, SF3 and SF5. The variation in the values of saturation magnetization exists because of different size and stoichiometric ratios of nanoparticles. When the size of nanoparticles is small contributes less superparamagnetic behavior [18]. It also shows that for SF3 and SF5, the observed hysteresis do not saturate at the maximum applied field. The saturation at maximum applied field for SC3 is 5 kOe. They were reproduced using ferromagnetic-like (FML) and superparamagnetic-like (SPL) contributions [8]. An F-center exchange (FCE) mechanism is employed to explain the ferromagnetism in Fe-doped SnO_2 nanocrystals, proposed by Coey et al. [26]. Such mechanism expects that Fe^{3+}–V_O^{2-}–Fe^{3+} groups will be common in the structure and an electron trapped in the oxygen

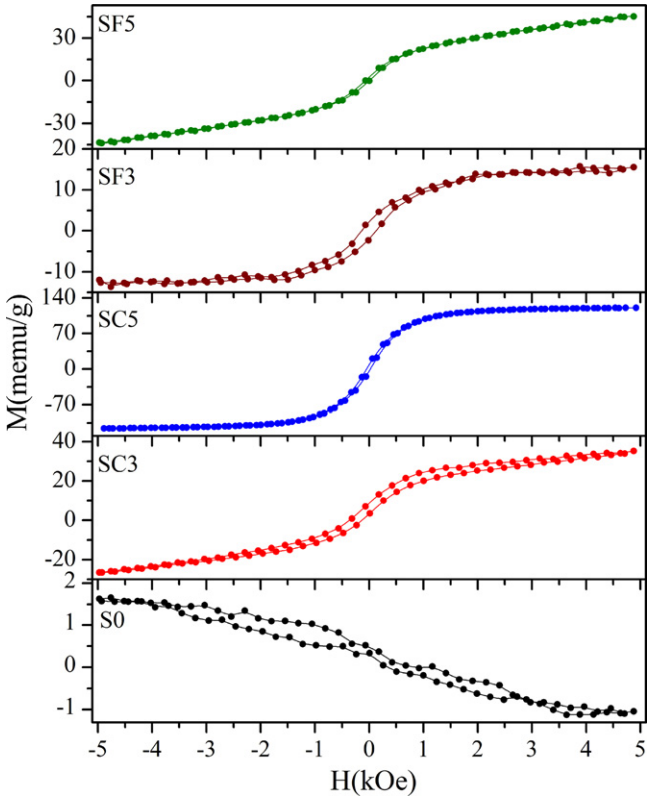

Fig. 7. Magnetization versus applied field (M–H) hysteresis curves.

vacancy makes an F center, where the electron occupies an orbital which overlaps the d shells of both iron neighbors. For ferric ions, $3d^5$ only has unoccupied minority spin orbitals, the trapped electron will be spin down, and the two iron neighbors will be spin up [26]. The exchange interaction between two irons via F center leads to the ferromagnetic coupling, where F center is similar to bound magnetic polaron. In addition, Fe^{3+} ion is paramagnetic and any Fe^{3+}–O–Fe^{3+} superexchange interactions will be antiferromagnetic (AF) in nature. Thus, the competition between ferromagnetic and paramagnetic/AF components will lead to the observed variations in saturation magnetization. In case of DMS nanoparticles, the interfacial oxygen vacancy (V_O^{2-}) defects between nanoparticles are believed to be essential for activating room-temperature or high-T_C ferromagnetism. According to this view, the interfacial defects are more easily formed and V_O^{2-} is probably favored due to the imperfect oriented attachment between the nanoparticles. This will promote the formation of Fe^{3+}–V_O^{2-}–Fe^{3+} groups between nanoparticles and benefit to FCE mechanism, resulting into improve ferromagnetism. Moreover, iron has a lower valence state than parent tin for which it substitute, so the dopants must influence the defect chemistry, which is also explained by Fitzgerald et al. [6]. The isolated oxygen vacancy captures an electron and forms F-center deep in the gap. The oxygen vacancies associated with the $3d$ dopants would be expected to trap the electrons. A suitable charge-compensating electronic defect is the replacement of a tin ion leads to ferromagnetic Fe^{2+} state from paramagnetic Fe^{3+} via

oxygen vacancies within Fe^{3+}–$V_O{}^{2-}$–Fe^{3+} group, is responsible for the ferromagnetism of Co and Fe doped SnO_2.

In the case of Co doped SnO_2 nanoparticles, the origin of ferromagnetism is very complex. Although different mechanisms might be responsible, an effort has been made to explain the phenomenon using the bound magnetic polarons (BMPs) model [26]. According to this model, the localized spins of the dopant ion interact with the charge carriers which are bound to a small number of defects such as oxygen vacancies, resulting in a magnetic polarization of the surrounding local moments. In the samples of present investigation, due to the substitution of Co for Sn, a number of free charge carriers and oxygen vacancies might have been introduced to maintain the charge neutrality leading to the formation of BMPs. The exchange interactions between these BMPs are coupled with the available small quantity of randomly distributed neighboring Co^{2+} might be responsible for the observed ferromagnetism.

Moreover, the room temperature ferromagnetism exists in the present samples because to the formation of small nano size particles [19]. The appearance of ferromagnetism is due to effective exchange interactions between the unpaired electrons spins originating from the surface defects such as oxygen vacancy clusters instead of single neutral oxygen vacancies associated with the nano metric size. Further, it is also important to note that during the annealing process, there may be a possibility of forming oxygen vacancy clusters due to the migration of oxygen vacancies, in addition to the removal of crystallized water or residual carbon. These oxygen vacancies not only influence the local structural disorder and surface morphology of the materials but also the distribution of Co and Fe ions which are incorporated in the host lattice and grain's structure. Moreover, during the heat treatment, the presence of residual organic impurities, concentration of surface defects, and their random distributions affect the local structural disorder and simultaneously, the grain growth would also occur. Thus not only the local structural disorder, oxygen vacancies, or vacancy clusters and their distribution but also the surface defects and their associated surface morphology of the samples have influenced the ferromagnetism.

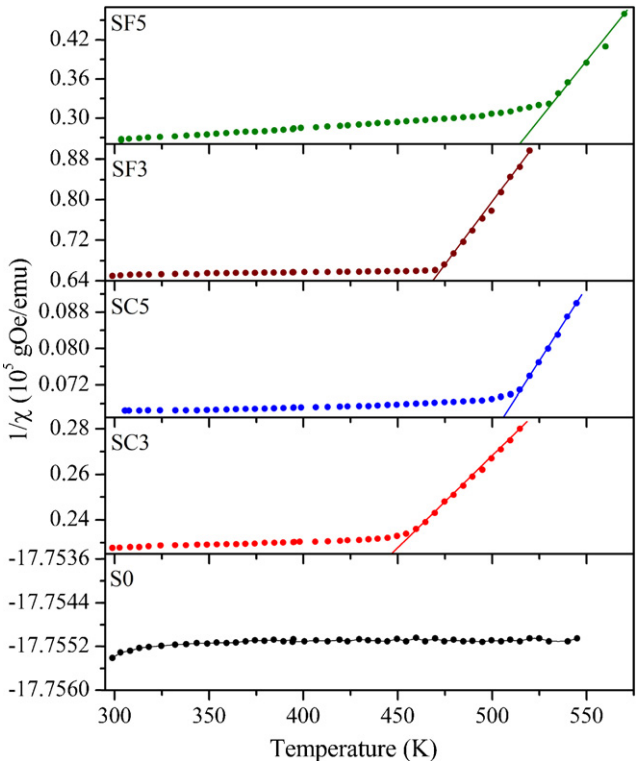

Fig. 8. Inverse of magnetic susceptibility ($\chi^{-1}(T)$) as the function of temperature with magnetizing field of 500 Oe.

Fig. 8 shows the variation of inverse susceptibility with temperature ($\chi^{-1}(T)$) in high-temperature regime of Co and Fe-doped SnO_2 nanoparticles with magnetizing field of 500 Oe. It is interesting to note that the magnetic susceptibility of S0 is negative because of its diamagnetic nature and it does not depend on temperature, whereas Co and Fe-doped samples show ferromagnetic behavior and exhibits strong temperature dependence, described by the Curie–Weiss law. The existence of ferromagnetic interactions is evident as χ^{-1} increases with the increasing temperature. We have extrapolated the fitted straight lines of χ^{-1} recorded in the high temperature region which indicated the magnetic phase transition temperature of 447, 505, 464 and 513 K for SC3, SC5, SF3 and SF5, respectively.

4. Conclusions

We have synthesized pure, Co and Fe-doped SnO_2 nanoparticles by a chemical route using polyvinyl alcohol as surfactant. The XRD results show the tetragonal rutile structure of pure and doped SnO_2 and the value of distortion ratio increases with increasing dopant concentration. The average particle size using FWHM is 12, 13, 21, 14 and 29 nm, respectively, for S0, SC3, SC5, SF3 and SF5 which is also confirmed by TEM images. FTIR spectra exhibit the characteristic signatures of SnO_2 of the Sn–O bond with absorption peaks between 430 and 620 cm^{-1}. The peaks corresponding to E_g, A_{1g} and B_{2g} of Raman shift show the formation of SnO_2 structure in each sample and the peaks near 428.64, 501.57, 768.79 and 860.06 cm^{-1} support the existence of nanosize particles. The PL spectra of the as-synthesized SnO_2 nanoparticles shows the optical nature and exhibits an intense blue luminescence at a wavelength of 531.13 nm which may be due to oxygen-related defects that have been introduced during the growth process. All the samples except S0 show room temperature ferromagnetism with nano size effect on the saturation magnetization. It has also been concluded that the magnetic properties depend not only on oxygen vacancies but also on electronic and structural modifications and surface nature of the nano crystallites. Ferromagnetic behavior is also explained on the basis of Curie Weiss law of ferromagnetism by temperature dependent magnetization with magnetizing field of 500 Oe.

References

[1] K. Nomura, H. Reuther, Nano-structure analysis of Fe implanted SnO_2 films by ^{57}Fe and ^{119}Sn CEMS, Journal of Nanoparticle Research 191 (2008) 159.

[2] Z.W. Chen, H.J. Zhang, Z. Li, Z. Jiao, M.H. Wu, C.H. Shek, C.M.L. Wu, J.K.L. Lai, Defect evolution of nanocrystalline SnO_2 thin films induced by pulsed delivery during in situ annealing, Acta Materialia 57 (2009) 5078.
[3] A. Punnoose, K.M. Reddy, J. Hays, A. Thurber, M.H. Engelhard, Magnetic gas sensing using a dilute magnetic semiconductor, Applied Physics Letters 89 (2006) 112509.
[4] P. Jajarmi, S. Barzegar, G.R. Ebrahimi, N. Varahram, Production of SnO_2 nano-particles by hydrogel thermal decomposition method, Materials Letters 65 (2011) 1249.
[5] S.B. Ogale, R.J. Choudhary, J.P. Buban, S.E. Lofland, S.R. Shinde, S.N. Kale, V.N. Kulkarni, J. Higgins, C. Lanci, J.R. Simpson, N.D. Browning, S.D. Sharma, H.D. Drew, R.L. Greene, T. Venkatesan, High temperature ferromagnetism with a giant magnetic moment in transparent Co-doped $SnO_{2-\delta}$, Physical Review Letters 91 (2003) 077205.
[6] C.B. Fitzgerald, M. Venkatesan, L.S. Dorneles, R. Gunning, P. Stamenov, J.M.D. Coey, P.A. Stampe, R.J. Kennedy, E.C. Moreira, U.S. Sias, Magnetism in dilute magnetic oxide thin films based on SnO_2, Physical Review B74 (2006) 115307.
[7] C.B. Fitzgerald, M. Venkatesan, A.P. Douvalis, S. Huber, J.M.D. Coey, SnO_2 doped with Mn, Fe or Co: room temperature dilute magnetic semiconductors, Journal of Applied Physics 95 (2004) 7390.
[8] A. Punnoose, J. Hays, A. Thurber, M.H. Engelhard, R.K. Kukkadapu, C. Wang, Development of high-temperature ferromagnetism in SnO_2 and paramagnetism in SnO by Fe doping, Physical Review B 72 (2005) 054402.
[9] R. Adhikari, A.K. Das, D. Karmakar, T.V.C. Rao, J. Ghatak, Structure and magnetism of Fe-doped SnO_2 nanoparticles, Physical Review B 78 (2008) 024404.
[10] S. Maensiri, J. Sree, C. Thomas, J. Klinkarwnarong, Magnetic behavior of nanocrystalline powders of Co-doped ZnO diluted magnetic semiconductors synthesized by polymerizable precursor method, Journal of Magnetism and Magnetic Materials 301 (2005) 422.
[11] A. Punnoose, J. Hays, V. Gopal, V. Shutthanandan, Room-temperature ferromagnetism in chemically synthesized $Sn_{1-x}Co_xO_2$ powders, Applied Physics Letters 85 (2004) 1559.
[12] A. Kar, M.A. Stroscio, M. Dutta, J. Kumari, M. Meyyappan, Observation of ultraviolet emission and effect of surface states on the luminescence from tin oxide nanowires, Applied Physics Letters 94 (2009) 101905.
[13] L.M. Fang, X.T. Zu, Z.J. Li, S. Zhu, C.M. Liu, L.M. Wang, F. Gao, Microstructure and luminescence properties of Co-doped SnO_2 nanoparticles synthesized by hydrothermal method, Journal of Nanoparticle Research 19 (2007) 868.
[14] X.T. Zhou, F. Heigl, M.W. Murphy, T.K. Sham, T. Regier, I. Coulthard, R.I.R. Blyth, Time-resolved X-ray excited optical luminescence from SnO_2 nanoribbons: direct evidence for the origin of the blue luminescence and the role of surface states, Applied Physics Letters 89 (2006) 213109.
[15] C. Fu, J. Wang, M. Yang, X. Su, J. Xu, B. Jiang, Effect of La doping on microstructure of SnO_2 nanopowders prepared by co-precipitation method, Journal of Non-Crystalline Solids 357 (2011) 1172.
[16] S. Su, R. Zuo, X. Wang, L. Li, Sintering, microstructure and piezoelectric properties of CuO and SnO_2 co-modified sodium potassium niobate ceramics, Materials Research Bulletin 45 (2010) 124.
[17] B. Sathyaseelan, K. Senthilnathan, T. Alagesan, R. Jayavel, K. Sivakumar, A study on structural and optical properties of Mn- and Co-doped SnO_2 nanocrystallites, Materials Chemistry and Physics 124 (2010) 1046.
[18] S. Ghosh, M. Mandal, K. Mandal, Effects of Fe doping Fe–N-codoping on magnetic properties of SnO_2 prepared by chemical co-precipitation, Journal of Magnetism and Magnetic Materials 323 (2011) 1083.
[19] K.C. Verma, R.K. Kotnala, N.S. Negi, Improved dielectric and ferromagnetic properties in Fe-doped $PbTiO_3$ nanoparticles at room temperature, Applied Physics Letters 92 (2008) 152902.
[20] J. Zhang, L. Gao, Synthesis and characterization of nanocrystalline tin oxide by sol–gel method, Journal of Solid State Chemistry 177 (2004) 1425.
[21] S. Emiroglu, N. Barsan, U. Weimaer, V. Hoffmann, In situ diffuse reflectance infrared spectroscopy study of CO adsorption on SnO_2, Thin Solid Films 391 (2001) 176.
[22] A. Dieguez, A.R. Rodriguez, A. Vila, J.R. Morante, The complete Raman spectrum of nanometric SnO_2 particles, Journal of Applied Physics 90 (2001) 1550.
[23] D.L. Hou, H.J. Meng, L.Y. Jia, X.J. Ye, H.J. Zhou, X.L. Li, Oxygen vacancy enhanced the room temperature ferromagnetism in Ni-doped TiO_2 thin films, Physics Letters A 364 (2007) 318.
[24] C.M. Liu, X.T. Zu, Q.M. Wei, L.M. Wang, Fabrication and characterization of wire-like SnO_2, Journal of Physics D: Applied Physics 39 (2006) 2494.
[25] F. Gu, S.F. Wang, C.F. Song, M.K. Lu, Y.X. Qi, G.J. Zhou, D. Xu, D.R. Yuan, Synthesis and luminescence properties of SnO_2 nanoparticles, Chemical Physics Letters 372 (2003) 451.
[26] J.M.D. Coey, A.P. Douvalis, C.B. Fitzgerald, M. Venkatesan, Ferromagnetism in Fe-doped SnO_2 thin films, Applied Physics Letters 84 (2004) 1332.